Semiclassical theory of shot noise in ballistic n^+-i-n^+ semiconductor structures: Relevance of Pauli and long-range Coulomb correlations

G. Gomila
Research Center for Bioelectronics and NanoBioScience, Departament d'Electrònica, Universitat de Barcelona, C/ Marti i Franques, 1, E-08028 Barcelona, Spain

I. R. Cantalapiedra
Departament de Física Aplicada, Universitat Politècnica de Catalunya, Av. Dr. Marañon, 44, E-08028 Barcelona, Spain

T. González
Departamento de Física Aplicada, Universidad de Salamanca, Plaza de la Merced, s/n, E-37008 Salamanca, Spain

L. Reggiani
INFM-National Nanotechnology Laboratory and Dipartimento di Ingegneria dell'Innovazione, Universitá di Lecce, Via Arnesano s/n, I-73100 Lecce, Italy

(Received 15 January 2002; revised manuscript received 22 April 2002; published 1 August 2002)

We work out a semiclassical theory of shot noise in ballistic n^+-i-n^+ semiconductor structures aiming at studying two fundamental physical correlations coming from Pauli exclusion principle and long-range Coulomb interaction. The theory provides a unifying scheme which, in addition to the current-voltage characteristics, describes the suppression of shot noise due to Pauli and Coulomb correlations in the whole range of system parameters and applied bias. The whole scenario is summarized by a phase diagram in the plane of two dimensionless variables related to the sample length and contact chemical potential. Here different regions of physical interest can be identified where only Coulomb or only Pauli correlations are active, or where both are present with different relevance. The predictions of the theory are proven to be fully corroborated by Monte Carlo simulations.

DOI: 10.1103/PhysRevB.66.075302 PACS number(s): 73.23.−b, 72.70.+m, 73.50.Td, 05.40.−a

I. INTRODUCTION

Ballistic conductors are characterized by an active region where carriers, once injected by contacts, move without suffering any scattering from contact to contact, i.e., the carrier mean free path is much longer than the sample characteristic dimensions. In metals, ballistic transport is usually studied in point contacts.[1] Such contacts allow the analysis of elastic and inelastic scattering processes by means of the so-called point contact spectroscopy.[2] Since the Fermi wavelength in metals is very small (~ 0.5 nm), the nature of carrier transport is semiclassical and quantum effects related to the wave nature of the electrons can be disregarded. In semiconductors, ballistic transport has been investigated in bulk materials,[3,4] point contacts,[5] and two-dimensional electron gases;[6] some studies have allowed the development of ballistic emission spectroscopy[7] for the analysis of semiconductor heterointerfaces. Moreover, a variety of ballistic electron devices with promising performances have been realized[8,9] or proposed.[10–12] Since the Fermi wavelength in semiconductors can be as large as 40 nm, the nature of the carrier transport can be either semiclassical or quantum depending on the characteristic sample dimensions, L, with respect to the Fermi wavelength, λ_F. For $\lambda_F \ll L$ transport is semiclassical, while for $\lambda_F \sim L$ transport is quantum.

From a fundamental point of view, the study of nonequilibrium electronic noise (shot noise)[13] of ballistic conductors in the semiclassical transport regime offers a unique scenario where the simultaneous effect of two fundamental physical interactions, namely the long-range Coulomb interaction and the Pauli exclusion principle, can be investigated. On the one hand, Pauli correlations have an influence on the carrier injecting statistics at the contacts. On the other hand, Coulomb correlations can modify the carrier passing statistics inside the active regions. The effect of both mechanisms results in values of the current noise below the full Poissonian value, i.e., in shot-noise suppression. Thus, the nonequilibrium low frequency current spectral density is given by $S_I(0) = \gamma 2qI$, with I being the current flowing through the sample and γ a dimensionless parameter (Fano factor) which takes values below unity because of the negative correlations induced by both mechanisms. The relative relevance of Coulomb and Pauli suppression in determining the Fano factor depends on parameters like the sample length, the temperature, the carrier density, or the applied voltage, thus allowing the monitoring of both correlation mechanisms.

The first theoretical analyses on the nonequilibrium noise properties of ballistic conductors were performed by Van der Ziel and Bosman in n^+-n^--n^+ ballistic semiconductor diodes[14] and by Kulik and Omel'yanchuk in ballistic metallic point contacts.[15] In the former case, by considering nondegenerate injection conditions, only the effect of the Coulomb correlations was evidenced. In particular, by using ideas borrowed from North's theory of vacuum tubes,[16] it was shown that under space charge conditions current noise results suppressed below the full Poissonian value (see also Refs. 17 and 18). In the latter case, the high carrier density of metals prevented the presence of significant space charge effects,

 ©2002 The American Physical Society

and hence the possibility to test the effect of the long-range Coulomb correlations. In this case, by means of a self-consistent semiclassical kinetic theory based on the Boltzmann–Langevin equation,[19] which included the effects of the Pauli principle, it was shown that in the collision free regime ballistic metallic point contacts displayed Nyquist noise with low frequency current spectral density given by $S_I(0)=4k_BT/R_S$, where k_B is the Boltzmann constant, T the temperature, and $R_S=mv_F/(q^2n)$ the Sharvin contact resistance, with m being the electron effective mass, v_F the Fermi velocity, q the unit charge, and n the carrier concentration inside the sample. This result is applied in the physical limit where $qV,k_BT\ll E_F$, and arbitrary relation between qV and k_BT, where V is the applied bias and E_F the Fermi energy. These initial studies did not allowed the study of the simultaneous effect of both Pauli and Coulomb correlation mechanisms.

It was only very recently that ballistic structures including the simultaneous effect of Pauli and Coulomb correlations have been analyzed.[20–22] By making use of a semianalytical approach,[20] Monte Carlo (MC) simulations,[21] and an asymptotic analytical approach,[22] nonequilibrium noise properties of ballistic semiconductor structures have been investigated. It was shown that these structures, by allowing both space charge effects and degenerate injection statistics, were unique in order to study the simultaneous effect of both Pauli and Coulomb correlations.[23] However, the existing studies, being valid only under some limit conditions or performed for some specific sets of system parameters, do not offer a complete overview of the relative relevance of Pauli and Coulomb correlations in the whole range of system parameters and applied bias. This lack of a general overview can prevent the designing of suitable experimental strategies to test the theoretical predictions. The aim of the present work is precisely to address this issue.

To this purpose we work out a general theory for the low frequency shot-noise properties of ballistic n^+-i-n^+ semiconductor diodes that also consistently describes current–voltage characteristics. We consider lightly doped bulk semiconductor materials since at low temperatures the bulk electrons are trapped by their parent donors, neutralizing them and thus minimizing both the $e-e$ interaction and ionized impurity scattering, thus allowing long mean free paths up to relatively high electron energies.[24,25] The theory presented accounts for both the Pauli exclusion principle and the long-range Coulomb interaction, and is applied to the whole range of system parameters (sample length, temperature, contact doping) and external bias. In particular, the theory allows us to study in a unifying framework the transition from: (i) nondegenerate to degenerate injection conditions, (ii) short to (asymptotically) long sample lengths and, (iii) low to (asymptotically) high applied voltages. By overcoming the limitations of the previous existing theories, the present study allows us to compress into a general scheme the full scenario displayed by the Pauli and Coulomb correlations in these ballistic structures. This scheme, validated and tested with a wide set of MC simulations, is believed to be of relevant assistance in designing future investigations on an experimental and/or simulation basis.

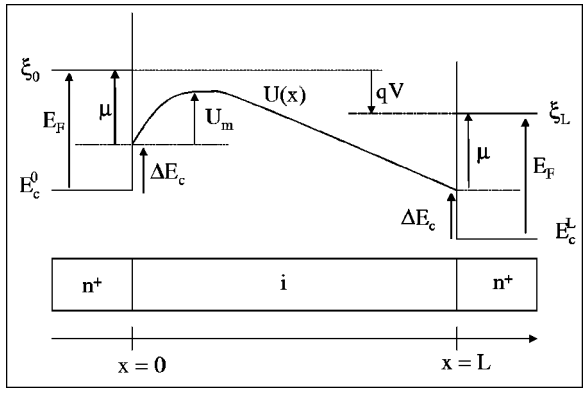

FIG. 1. Schematic band diagram of the ballistic structure under study.

The paper is organized as follows. In Sec. II we describe the system under study. In Sec. III we present the physical model used to analyze the nonequilibrium noise properties. In Sec. IV the analytical expressions obtained for the transport and noise properties are reported, and their validity is checked by means of MC simulations. In Sec. V we propose a general scheme able to provide a systematic physical picture of the shot-noise properties of two-terminal ballistic conductors, and check its reliability by means of the developed theory. Finally, in Sec. VI we summarize the main results of the paper. The Appendix is devoted to technical derivations.

II. SYSTEM UNDER STUDY

The system under study is the n^+-i-n^+ ballistic semiconductor diode shown in Fig. 1. It consists of an undoped semiconductor of length L, where injected carriers move in the total absence of scattering events, sandwiched between two highly doped regions which act as ideal injecting contacts as specified later. The contacts and the ballistic region are taken of the same material (homodiode) or of different material (heterodiode). In the former case the band offset $\Delta E_c \equiv U(0)-E_c^0=U(L)-E_c^L$ (a symmetric structure is assumed for simplicity) vanishes, while in the latter case it takes a finite value. The ballistic region is taken to be perfectly coupled with the contacts, thus no reflections take place at the interfaces. The contacts are assumed to be in quasiequilibrium at the given temperature, and at electrochemical potentials ξ_0 and ξ_L, with $\xi_L-\xi_0=qV$. The voltage drop in the contacts is assumed to be negligibly small (Ohmic contacts), and hence all the band bending occurs in the active region of the sample. Under these assumptions, the effective contact chemical potential μ, defined as $\mu\equiv\xi_0-U(0)=\xi_L-U(L)$, is independent of the applied bias. Note that for the case of an homodiode μ coincides with the contact Fermi energy, $E_F\equiv\xi_0-E_c^0=\xi_0-E_c^L$, while for the case of an heterodiode one has $\mu=E_F-\Delta E_c$. We note the existence of a maximum with amplitude U_m in the potential energy along the active region due to the presence of space charge. The structure is assumed to be sufficiently thick in the transversal directions so as to allow for a one-dimensional (1D) electrostatic treatment. Thus the system is 1D in real space and three-

dimensional (3D) in momentum space.[18] The carriers are injected into the active region in accordance with the equilibrium Fermi–Dirac distribution function and satisfying the Pauli exclusion principle, thus following the corresponding binomial injection statistics.[26,27] For simplicity, a single spherical parabolic band is assumed.

The parameters describing the above-introduced model system are therefore the length of the conductor, L, the cross-sectional area A, the effective contact chemical potential, μ, the temperature, T, the static dielectric constant of the medium, ϵ, the electron effective mass, m, and the charge carriers q. The independent-variable parameter is the applied voltage, V.

As mentioned previously, the correlations between different current pulses in the present system is twofold. On the one hand, Pauli correlations have an influence on the contact injecting statistics. Carriers above the Fermi energy, at the tail of the Fermi distribution at the contacts, are injected obeying Poissonian statistics due to the negligible influence of the Pauli principle at such high energies. Carriers near and below the Fermi energy are injected following a binomial (sub-Poissonian) statistics due to the increasing influence of the Pauli principle at the highly occupied states. On the other hand, Coulomb correlations, through the potential energy maximum U_m associated with the presence of space charge, can modify the carrier passing statistics inside the active region. Indeed, the fluctuations of U_m originated by the passage of carriers over the maximum modulate the transmission of further carriers (spacing them out more regularly in time) and smooth out the current fluctuations imposed by the random injection at the contacts. The relative importance of the two types of correlating mechanisms depends on the values of L, μ, and V.

III. PHYSICAL MODEL

Within a semiclassical approach the description of the transport and noise properties of the system under study can be carried out by means of the Vlasov equation, self-consistently coupled to the Poisson equation, and supplemented by appropriate *fluctuating* boundary conditions.[19] In the one-dimensional approximation followed here, the Vlasov–Poisson system of equations reads (in dimensionless units, as specified later):

$$\left[\frac{\partial}{\partial t}+v_x\frac{\partial}{\partial x}-\frac{\partial U(x,t)}{\partial x}\frac{\partial}{\partial v_x}\right]F(x,v_x,t)=0, \tag{1}$$

$$\frac{\partial^2 U(x,t)}{\partial x^2}=-n(x,t), \tag{2}$$

$$n(x,t)=\int_{-\infty}^{+\infty}dv_x F(x,v_x,t), \tag{3}$$

where t is the time variable, x the spatial coordinate, v_x the velocity in the x direction, $U(x,t)$ the potential energy, $F(x,v_x,t)$ the distribution function integrated over transversal momentum directions, and $n(x,t)$ the carrier density. In the Poisson equation the contribution of the intrinsic free carrier density is neglected in comparison to the injected carriers. Moreover, the boundary conditions for the potential energy read

$$U(0,t)\equiv U_0=0, \quad U(L,t)\equiv U_L=V, \tag{4}$$

where we have assumed that the applied bias is fixed by a low impedance external circuit so that neither the electric potential nor the contact potential energies fluctuates, i.e., $\delta U_0(t)=\delta U_L(t)=\delta V(t)=0$. Accordingly, the boundary conditions for the distribution function at the contacts read:

$$F(0,v_x,t)=\overline{F}(v_x)+\delta F_0(v_x,t), \quad v_x>0, \tag{5}$$

$$F(L,v_x,t)=\overline{F}(v_x)+\delta F_L(v_x,t), \quad v_x<0. \tag{6}$$

These boundary conditions consist of two contributions. The first is of deterministic nature, and gives the average value of the distribution function. The second is of stochastic nature, and describes the random injection of carriers. The average distribution function is given by

$$\begin{aligned}\overline{F}(v_x)&=\int_0^{+\infty}d\varepsilon_\perp f_{\mathrm{FD}}(\varepsilon_\perp+\varepsilon_x-\mu)\\&=\ln(1+e^{-\varepsilon_x+\mu})\equiv f_c(\varepsilon_x-\mu),\end{aligned} \tag{7}$$

with $\varepsilon_x=\frac{1}{2}v_x^2$ and $\varepsilon_\perp=\frac{1}{2}v_\perp^2$ being the longitudinal and transversal kinetic energy, respectively, and where

$$f_{\mathrm{FD}}(\varepsilon)=\frac{1}{1+e^{\varepsilon}} \tag{8}$$

is the Fermi–Dirac distribution function. Note that due to the integration over the transverse momentum directions the effective one-dimensional contact distribution function is $f_c(\varepsilon)$ instead of $f_{\mathrm{FD}}(\varepsilon)$. Moreover, the fluctuating contributions $\delta F_0(v_x,t)$ and $\delta F_L(v_x,t)$ have zero mean and low frequency spectral density given by[22]

$$\begin{aligned}2\int_{-\infty}^{+\infty}&\overline{\delta F_a(v_x,t)\,\delta F_{a'}(v_x',t')}dt\\&=\frac{\partial f_c(\varepsilon_x-\mu)}{\partial\mu}\delta_{a,a'}\delta(\varepsilon_x-\varepsilon_x')\delta(t-t')\\&=f_{\mathrm{FD}}(\varepsilon_x-\mu)\delta_{a,a'}\delta(\varepsilon_x-\varepsilon_x')\delta(t-t').\end{aligned} \tag{9}$$

Equations (1)–(9) constitute the complete set of equations to study the noise properties of the ballistic structure described in Sec. II.

In the previous set of equations, and in what follows, we use dimensionless variables to simplify the notation. The dimensionalizing factors used for energy, length, carrier density, velocity, distribution function, electric potential, electric field, electric current, resistance, and current spectral density are, respectively,

$$U_0=k_BT,\quad L_0=\sqrt{\frac{\epsilon k_BT}{q^2N_0}},\quad N_0=4\pi\frac{(mk_BT)^{3/2}}{h^3},$$

$$v_0=\left(\frac{k_BT}{m}\right)^{1/2},\quad F_0=\frac{N_0}{v_0},\quad V_0=\frac{k_BT}{q},\tag{10}$$

$$E_0=\sqrt{\frac{N_0k_BT}{\epsilon}},\quad I_0=qAN_0v_0,\quad R_0=\frac{V_0}{I_0},\quad S_{I_0}=2qI_0,$$

where h is the Planck constant. With these dimensionalizing factors the dimensionless parameters describing the system are $L/L_0\rightarrow L$ and $\mu/k_BT\rightarrow\mu$, and the dimensionless independent variable is $qV/k_BT\rightarrow V$. The physical meaning of the different parameters is the following: N_0 is the effective density of states in the conduction band, L_0 is the Debye screening length associated to N_0, U_0 is the thermal energy, v_0 is the thermal velocity, V_0 is the thermal voltage, E_0 the thermal electric field, I_0 the current associated to N_0 and v_0, R_0 the resistance associated to V_0/I_0, and S_{I_0} the shot noise level associated to I_0.

To complete our analysis, we will perform MC simulations of the system under study, so that the validity of the analytical theory can be checked by comparison. To this end we use an ensemble MC simulator, 3D in momentum space and self-consistently coupled with a 1D Poisson solver to account for Coulomb interaction. The carrier dynamics is simulated in the ballistic active region of the structure and the electron injection from the thermal reservoirs is modeled according to Fermi statistics. Due to the Pauli principle, the instantaneous occupancy of an incoming electron state with energy ε and impinging at the interface between the ideal thermal reservoir and the active region fluctuates in time obeying a binomial distribution[26] with a probability of success given by $f_{\rm FD}(\varepsilon-\mu)$. This statistic is implemented in the MC simulation of the contact injection by introducing a discretization of momentum space and using the rejection technique to select the times of injection at every momentum state.[27] As limiting cases, when $\varepsilon-\mu\ll-1$, $f_{\rm FD}(\varepsilon-\mu)\cong1$ and the injection statistic of the corresponding state is uniform in time. By contrast, when $\varepsilon-\mu\gg1$, $f_{\rm FD}(\varepsilon-\mu)\ll1$ and the injection statistic is Poissonian. For the calculations we use the following parameters: $T=300$ K, $m=0.25\ m_0$, $\epsilon=11.7\ \epsilon_0$, with m_0 the free electron mass and ϵ_0 the vacuum permittivity.

IV. ANALYTICAL SOLUTION

The low frequency solution of the model presented in Sec. III can be obtained in fully analytical form. For the sake of conciseness, in the following we only present the final expression of the relevant quantities of interest and refer to the Appendix for the details of the derivation.

A. $I-V$ characteristics and steady-state profiles

Following the results presented in Appendix, the current voltage (I–V) characteristics of the ballistic conductor presented in Sec. II can be calculated as

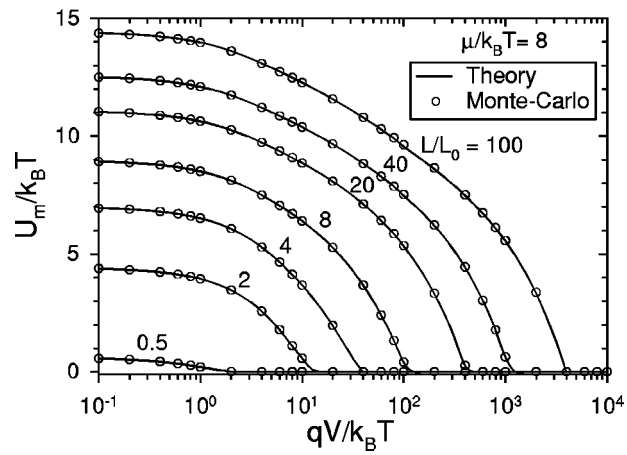

FIG. 2. Maximum energy potential $\overline{U}_m/k_BT$ as a function of voltage for $\mu/k_BT=8$ and several values of the sample length L/L_0. Solid line refers to the result of the analytical calculations and open circles to those of the MC simulations.

$$\overline{I}=\int_{\overline{U}_m}^{+\infty}du[f_c(u-\xi_L)-f_c(u-\xi_0)],\tag{11}$$

where $f_c(\varepsilon)$ is given in Eq. (7), $\overline{U}_m$ is the average value of the maximum potential energy at applied bias V, and $\xi_L=V+\mu$ and $\xi_0=\mu$ are the electrochemical potentials at the contacts located at $x=L$ and $x=0$, respectively. The value of $\overline{U}_m$ can be calculated through (see the Appendix)

$$L=\int_{\overline{U}_0}^{\overline{U}_m}\frac{dU}{E^-(U,\overline{U}_m)}-\int_{\overline{U}_L}^{\overline{U}_m}\frac{dU}{E^+(U,\overline{U}_m)},\tag{12}$$

where

$$E^-(U,\overline{U}_m)=\left\{\int_{\overline{U}_m}^{\infty}du[\sqrt{u-U}-\sqrt{u-\overline{U}_m}]\times[f_c(u-\xi_L)+f_c(u-\xi_0)]+\int_U^{\overline{U}_m}du\sqrt{u-U}2f_c(u-\xi_0)\right\}^{1/2}2^{3/4}\tag{13}$$

and

$$E^+(U,\overline{U}_m)=-\left\{\int_{\overline{U}_m}^{\infty}du[\sqrt{u-U}-\sqrt{u-\overline{U}_m}]\times[f_c(u-\xi_L)+f_c(u-\xi_0)]+\int_U^{\overline{U}_m}du\sqrt{u-U}2f_c(u-\xi_L)\right\}^{1/2}2^{3/4}.\tag{14}$$

Figure 2 reports the maximum potential energy as a function of the voltage, as calculated from Eq. (12) with $\mu=8$ at different values of the sample length. MC results are also shown. Excellent agreement is found between analytical and MC calculations. At vanishing voltages $\overline{U}_m$ saturates at higher values the longer the normalized length, because of

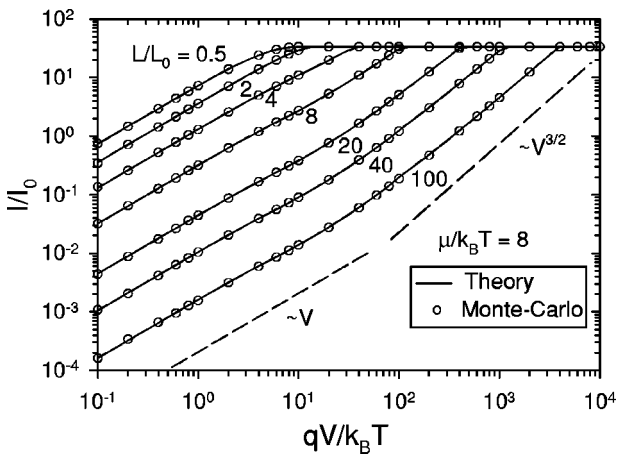

FIG. 3. $I-V$ characteristics for $\mu/k_BT=8$ and several values of the sample length L/L_0. Solid lines refer to the result of the analytical calculations and open circles to those of MC simulations. Dashed curves indicate the typical power law behaviors of the Ohmic (V) and Child–Langmuir ($V^{3/2}$) regimes.

the increasing effect of space charge inside the ballistic region. At increasing voltages $\overline{U}_m$ starts decreasing until vanishing at a threshold voltage V_{cr}^m.

Figure 3 shows the $I-V$ characteristics as calculated from Eq. (11) for $\mu=8$ and several sample lengths. Figure 3 also reports the results of MC simulations. We have found perfect agreement between the results of the theory and those of MC simulations as expected, since both results are exact solutions of the same physical model. The main features of the $I-V$ characteristics consist in the presence of a linear (Ohmic) behavior at low applied voltages and a current saturation regime at high voltages. The resistance of the linear regime is given by (in dimensionless units)

$$R_{\rm eq}=\frac{1}{f_c(\overline{U}_m^{eq}-\mu)}. \tag{15}$$

In general, this value depends on both the sample length L and the reduced chemical potential μ. When $\overline{U}_m^{eq}\ll|\mu|$ the resistance takes a value independent of the sample length $R_{\rm eq}^{univ}=1/f_c(-\mu)$ in agreement with the results of Ref. 28. Typically this happens for $L\ll 5$ and $\mu\gg 5$, which represent the conditions for negligible space charge inside the ballistic region. In this limit, and when $\mu\gg 1$, $R_{\rm eq}^{univ}$ tends to the Sharvin contact resistance R_S. The value of the saturation current is given by (in dimensionless units)

$$I_{sat}=\int_0^{+\infty} f_c(u-\mu)du. \tag{16}$$

Current saturation takes place when all carriers injected from one contact reach the opposite one, while none of the carriers injected from the other contact is able to cross the ballistic region. The value of the saturation current is independent of the sample length since it is only determined by the emission properties of the contacts. The voltage for the onset of current saturation, V_{cr}, depends on both L and μ, as can be seen in Fig. 3. In the case that $\mu>V_{cr}^m$, where V_{cr}^m is the bias value at which the maximum of the potential energy disappears (see Fig. 2), one has $V_{cr}\cong\mu+3$. Otherwise, when $\mu<V_{cr}^m$, one has $V_{cr}=V_{cr}^m$, and saturation coincides with the disappearance of the maximum of the potential energy. Between the linear and the current saturation regimes the $I-V$ characteristic displays a nonlinear region, whose properties are determined by the precise values of L and μ. The asymptotic behavior of this nonlinear region for large values of L in the limit when $\overline{U}_m\ll V<V_{cr}$ consists of a slightly sublinear region followed by a superlinear characteristic of Child–Langmuir type[29] $I_{CL}=V^{3/2}/L^2$, as has been found in Ref. 22. The sublinear region is associated with a nonzero temperature value which smooths out the Fermi distribution. The superlinear region is associated with space-charge effects driven by the presence of U_m.

The steady state profiles can also be calculated in closed analytical form. The potential energy profile can be obtained in inverse form from the following relations (see the Appendix):

$$\int_{U_0}^{\overline{U}^-(x)}\frac{dU}{E^-(U,\overline{U}_m)}=x,\quad 0<x<\overline{x}_m, \tag{17}$$

$$\int_{U_L}^{\overline{U}^+(x)}\frac{dU}{E^+(U,\overline{U}_m)}=x-L,\quad \overline{x}_m<x<L, \tag{18}$$

where $\overline{x}_m$ is the location of the potential energy maximum inside the ballistic region. The value of $\overline{x}_m$ can be calculated from either Eq. (17) or Eq. (18) by setting the value of $\overline{U}(x)$ equal to $\overline{U}_m$. Once the potential energy profile is obtained, the electric field profile can be calculated as (see the Appendix)

$$\overline{E}(x)=\begin{cases} E^-[\overline{U}^-(x),\overline{U}_m], & 0<x<\overline{x}_m \\ E^+[\overline{U}^+(x),\overline{U}_m], & \overline{x}_m<x<L, \end{cases} \tag{19}$$

where $E^-(U,U_m)$ and $E^+(U,U_m)$ are given in Eqs. (13) and (14), respectively. Finally, the carrier density profile is obtained from (see the Appendix)

$$\overline{n}(x)=\begin{cases} \displaystyle\int_{\overline{U}_m}^{+\infty}\frac{du}{\sqrt{2[u-\overline{U}^-(x)]}}[f_c(u-\xi_0)+f_c(u-\xi_L)] \\ \displaystyle+\int_{\overline{U}^-(x)}^{\overline{U}_m}\frac{du}{\sqrt{2[u-\overline{U}^-(x)]}}2f_c(u-\xi_0);\quad 0<x<\overline{x}_m \\ \displaystyle\int_{\overline{U}_m}^{+\infty}\frac{du}{\sqrt{2[u-\overline{U}^+(x)]}}[f_c(u-\xi_0)+f_c(u-\xi_L)] \\ \displaystyle+\int_{\overline{U}^+(x)}^{\overline{U}_m}\frac{du}{\sqrt{2[u-\overline{U}^+(x)]}}2f_c(u-\xi_L);\quad \overline{x}_m<x<L. \end{cases} \tag{20}$$

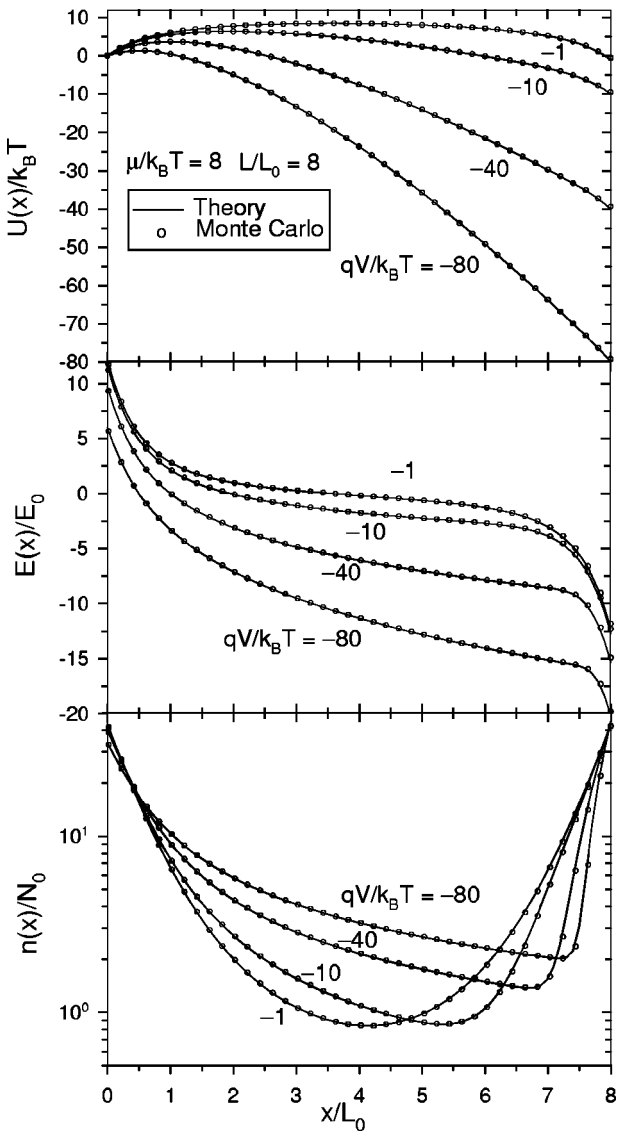

FIG. 4. Steady state profiles of the potential energy $U(x)/k_BT$, electric field $E(x)/E_0$, and carrier density $n(x)/N_0$ for $\mu/k_BT=8$ and $L/L_0=8$, at different values of the applied voltage qV/k_BT. Solid lines refer to the results of analytical calculations, open circles to those of MC simulations.

Figure 4 reports the steady state profiles for $\mu=8$ and $L=8$, at several values of the applied bias. For the sake of comparison, Fig. 4 also reports the profiles obtained from MC simulations. Again analytical calculations are found to perfectly agree with the simulations. Figure 4 clearly illustrates the space-charge nature of the transport and the presence of the potential energy maximum. The value of the potential energy maximum decreases systematically at increasing bias (as already indicated in Fig. 2), while its location shifts toward the left contact. At the same time, the free charge redistributes inside the structure by shifting the minimum of the carrier density from the center of the sample towards the right contact.

B. Noise properties

The low frequency noise properties of the system under study are characterized by the low frequency spectral density of current fluctuations defined as (in dimensionless units)

$$S_I(0)=\int_{-\infty}^{+\infty}\overline{\delta I(0)\delta I(t)}dt. \tag{21}$$

When interested in the study of the microscopic correlations the proper figure of merit is the Fano factor γ, which is obtained from $S_I(0)$ as (in the dimensionless units)

$$\gamma=\frac{S_I(0)}{\overline{I}}. \tag{22}$$

For conditions far from thermal equilibrium ($V>3$) a value of $\gamma=1$ corresponds to the absence of correlations between different current pulses, while $\gamma<1(\gamma>1)$ corresponds to the presence of negative (positive) correlations.

As shown in the Appendix, $S_I(0)$ can be calculated in closed analytical form for the model presented in Sec. III. The final result can be written in the following compact form (see the Appendix):

$$S_I(0)=\int_{\overline{U}_L}^{+\infty}du[\gamma_L(u)]^2 f_{\rm FD}(u-\xi_L)+\int_{\overline{U}_0}^{+\infty}du[\gamma_0(u)]^2 f_{\rm FD}(u-\xi_0), \tag{23}$$

where (see the Appendix)

$$\gamma_L(u)=\begin{cases}1+\Omega\tilde{\gamma}^{>}(u), & \overline{U}_m<u<+\infty\\ \Omega\tilde{\gamma}_L^{<}(u), & \overline{U}_L<u<\overline{U}_m,\end{cases} \tag{24}$$

$$\gamma_0(u)=\begin{cases}-1+\Omega\tilde{\gamma}^{>}(u), & \overline{U}_m<u<+\infty\\ \Omega\tilde{\gamma}_0^{<}(u), & \overline{U}_0<u<\overline{U}_m.\end{cases} \tag{25}$$

Here, we have defined

$$\Omega=-\frac{[\overline{f}_c(\overline{U}_m-\xi_L)-\overline{f}_c(\overline{U}_m-\xi_0)]}{\Delta}, \tag{26}$$

with

$$\Delta=\frac{1}{\overline{E}_0}-\frac{1}{\overline{E}_L}+\int_{\overline{U}_L}^{\overline{U}_m}du\,\tilde{\gamma}_L^{<}(u)\overline{f}_{\rm FD}(u-\xi_L)+\int_{\overline{U}_0}^{\overline{U}_m}du\,\tilde{\gamma}_0^{<}(u)\overline{f}_{\rm FD}(u-\xi_0)+\int_{\overline{U}_m}^{+\infty}du\,\tilde{\gamma}^{>}(u)[\overline{f}_{\rm FD}(u-\xi_0)+\overline{f}_{\rm FD}(u-\xi_L)]. \tag{27}$$

Moreover,

$$\tilde{\gamma}^{>}(u)=\int_{\overline{U}_0}^{\overline{U}_m}dU\frac{\sqrt{2(u-U)}-\sqrt{2(u-\overline{U}_m)}}{E^-(U,\overline{U}_m)^3}-\int_{\overline{U}_L}^{\overline{U}_m}dU\frac{\sqrt{2(u-U)}-\sqrt{2(u-\overline{U}_m)}}{E^+(U,\overline{U}_m)^3}, \tag{28}$$

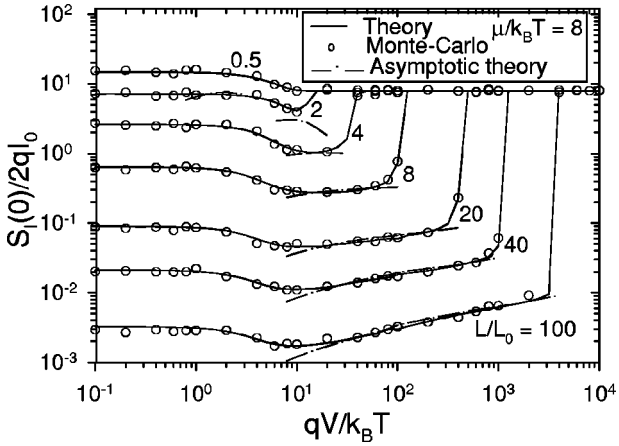

FIG. 5. Low frequency current spectral density $S_I(0)/2qI_0$ as a function of the applied voltage qV/k_BT for $\mu/k_BT=8$ and several values of the sample length L/L_0. Solid lines refer to the results of analytical calculations, open circles to those of MC simulations. Dot-dashed lines are the results of the asymptotic theory (Ref. 22).

$$\tilde{\gamma}_L^<(u)=-2\int_{\overline{U}_L}^{u} dU \frac{\sqrt{2(u-U)}}{E^+(U,\overline{U}_m)^3}, \tag{29}$$

$$\tilde{\gamma}_0^<(u)=2\int_{\overline{U}_0}^{u} dU \frac{\sqrt{2(u-U)}}{E^-(U,\overline{U}_m)^3}. \tag{30}$$

From the previous equations we can evaluate $S_I(0)$ and, in turn, the Fano factor γ. Note that these analytical expressions are valid in the whole range of system parameters L and μ, and in the whole range of applied bias V.

For the purpose of a reliability test, the results obtained from the analytical formulas are compared with those of MC simulations in Fig. 5. Here, the low frequency current spectral density is reported as a function of applied bias for $\mu=8$ and several sample lengths. As can be seen in Fig. 5, the agreement between the analytical theory and MC simulations is excellent, thus proving the reliability of both theory and simulations. For the sake of completeness Fig. 5 also reports the results obtained by means of the asymptotic theory developed in Ref. 22. According to this theory, in the limit of $\overline{U}_m \ll V < V_{cr}$ the low frequency current spectral density can be approximated by (in dimensionless variables)

$$S_I^{asym}=\beta(\mu-\overline{U}_m)\frac{I}{V+\overline{U}_m}, \tag{31}$$

with

$$\beta(\alpha)=9\left(1-\frac{\pi}{4}\frac{[F_{1/2}(\alpha)]^2}{F_0(\alpha)F_1(\alpha)}\right), \tag{32}$$

where $F_j(\alpha)=1/\Gamma(j+1)\int_0^\infty dy\, y^j f_{\rm FD}(y-\alpha)$, with $\Gamma(z)$ being the gamma function. As seen in Fig. 5 the asymptotic theory agrees well with the present theory for $\overline{U}_m \ll V < V_{cr}$. However, it cannot describe either the transition between low and high bias regions, or the case of small sample lengths in which the condition $\overline{U}_m \ll V < V_{cr}$ cannot be satisfied.

The main features of the low frequency spectral density depicted in Fig. 5 are summarized as follows. At low voltages ($V<3$), where Ohmic conditions are satisfied, $S_I(0)$ is bias independent and takes the value (in dimensionless variables)

$$S_I^{eq}(0)=\frac{2}{R_{\rm eq}}=2f_c(\overline{U}_m^{eq}-\mu), \tag{33}$$

in agreement with Nyquist theorem.[30] At high voltages ($V>V_{cr}$), when the sample exhibits current saturation conditions, $S_I(0)$ is again bias independent and given by (in dimensionless variables)

$$S_I^{sat}(0)=\int_0^{+\infty} du f_{\rm FD}(u-\xi_0)=f_c(-\mu). \tag{34}$$

In the region of intermediate values of voltages, $S_I(0)$ can present a monotonic or a nonmonotonic behavior (with the presence of a minimum) determined by the interplay between Coulomb and Pauli correlations, as will be detailed in Sec. V.

V. THE SCENARIO OF SHOT-NOISE IN BALLISTIC n^+-i-n^+ STRUCTURES

The present theory enables us to investigate separately the relevance of the two mechanisms responsible for the correlations in the system under study, namely, the Pauli exclusion principle and the long-range Coulomb interaction, in the whole range of system parameters. Accordingly, we propose a general scheme which summarizes the whole scenario of the shot-noise properties exhibited by n^+-i-n^+ ballistic semiconductor structures. To construct such a scheme, we make use of the Fano factor, γ, which is factorized into the two independent contributions, γ_P and γ_C, related to the Pauli and Coulomb correlations, respectively. Indeed, according to Eq. (9), the fluctuations of the contact distribution function at different energy levels are uncorrelated, so that the only source of correlations among carriers injected with different energy is the Coulomb interaction in the active region. As a consequence, both contributions to the Fano factor are independent, which implies $\gamma=\gamma_P\gamma_C$. Thus, the Pauli contribution γ_P corresponds to the Fano factor that would be obtained in the absence of the self-consistent long-range Coulomb interaction. It can be easily evaluated from the noise calculation performed in the Appendix by neglecting the self-consistent contribution. This is equivalent to the setup in Eq. (23),

$$\gamma_L(u)=\begin{cases}1, & \overline{U}_m<u<+\infty\\ 0, & \overline{U}_L<u<\overline{U}_m,\end{cases} \tag{35}$$

$$\gamma_0(u)=\begin{cases}-1, & \overline{U}_m<u<+\infty\\ 0, & \overline{U}_0<u<\overline{U}_m.\end{cases} \tag{36}$$

For the current spectral density associated with Pauli correlations only, it is thus obtained

$$S_I^P(0)=f_c(\overline{U}_m-\xi_L)+f_c(\overline{U}_m-\xi_0), \tag{37}$$

so that the Pauli contribution to the Fano factor is found to be

$$\gamma_P=\frac{S_I^P(0)}{\overline{I}}=\frac{f_c(\overline{U}_m-\xi_L)+f_c(\overline{U}_m-\xi_0)}{\int_{\overline{U}_m}^{+\infty}du[f_c(u-\xi_L)-f_c(u-\xi_0)]}, \tag{38}$$

where use is made of Eq. (11).

The Coulomb contribution is then evaluated as $\gamma_C=\gamma/\gamma_P$. According to these definitions, for $V>3$ values of $\gamma_P\neq 1$ correspond to the presence of Pauli correlations, while values of $\gamma_C\neq 1$ correspond to the presence of Coulomb correlations.

A detailed analysis of Eq. (38) indicates that the Pauli contribution is essentially dependent on the difference $\overline{U}_m-\mu$. Hence, when $\overline{U}_m-\mu>0$ it is $\gamma_P\rightarrow 1$, thus indicating the absence of Pauli correlations. In particular, for nondegenerate injection conditions $\mu<0$, one always has that $\overline{U}_m-\mu>0$, hence indicating the absence of Pauli correlations, as should be. By contrast, when $\overline{U}_m-\mu<0$ it is $\gamma_P<1$, thus indicating the presence of Pauli correlations. Since $\overline{U}_m$ is a decreasing function of the bias, the condition $\overline{U}_m^{eq}-\mu<0$ implies automatically that the inequality $\overline{U}_m-\mu<0$ is satisfied for all bias values, and hence the presence of Pauli correlations for $V>3$. On the contrary, when $\overline{U}_m^{eq}-\mu>0$ Pauli correlations are absent for low (or intermediate) bias values and present for bias values sufficiently high to validate the condition $\overline{U}_m-\mu<0$.

Concerning Coulomb correlations, their presence or absence is roughly determined by a value of the ratio L/L_{D_c} higher or lower than unity, respectively, where L_{D_c} is the Debye screening length corresponding to an homogeneous system with charge density equal to the equilibrium contact density. Taking into account the effects of degenerancy, L_{D_c} is calculated as (in dimensionless variables)

$$L_{D_c}=\left(\frac{dn_c^{eq}}{d\mu}\right)^{-1/2}=\frac{1}{\sqrt{2\int_0^{+\infty}du\,\frac{f_{\mathrm{FD}}(u-\mu)}{\sqrt{2u}}}}, \tag{39}$$

where we used that from Eq. (20) one has

$$n_c^{eq}=\overline{n}^{eq}(0)=2\int_0^{+\infty}du\,\frac{f_c(u-\mu)}{\sqrt{2u}}. \tag{40}$$

On the basis of these considerations, for the scenario of the shot-noise properties in ballistic conductors we propose the general scheme displayed in Fig. 6. In this scheme we identify five different regions in the plane (L,μ), corresponding to five different possibilities of interplay between Coulomb and Pauli correlations. The different regions in Fig. 6 are determined by the three lines defined by the equalities $L=L_{D_c}$, $\mu=0$, and $\mu=\overline{U}_m^{eq}$.

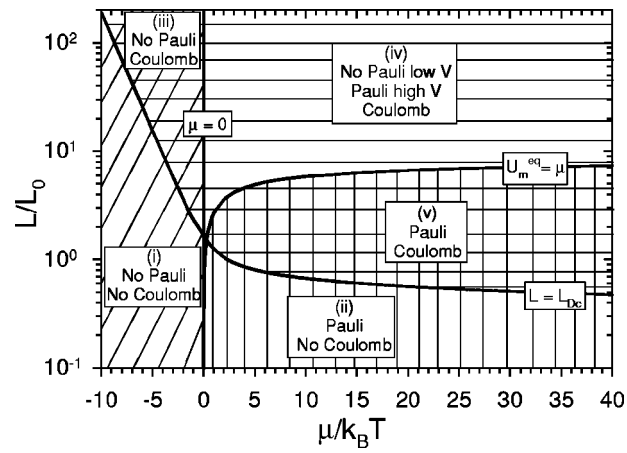

FIG. 6. Parameter plane in the length /chemical potential space representing the five different behaviors of the shot-noise properties of a ballistic conductor according to the relevance of the Pauli and Coulomb correlations. The three continuous lines define, respectively, the equalities: $L=L_{D_c}$, $\mu=0$, and $\overline{U}_m^{eq}=\mu$.

The shot-noise behavior in each of the five regions corresponds, respectively, to: (i) the absence of both Pauli and Coulomb correlations ($\mu<0$ and $L/L_{D_c}<1$); (ii) the presence of Pauli correlations and the absence of Coulomb correlations ($\mu>0$, $\overline{U}_m^{eq}-\mu<0$, and $L/L_{D_c}<1$); (iii) the absence of Pauli correlations and the presence of Coulomb correlations ($\mu<0$ and $L/L_{D_c}>1$); (iv) the absence (presence) of Pauli correlations for low (high) bias and the presence of Coulomb correlations ($\mu>0$, $\overline{U}_m^{eq}-\mu>0$, and $L/L_{D_c}>1$); (v) the presence of both Pauli and Coulomb correlations ($\mu>0$, $\overline{U}_m^{eq}-\mu<0$, and $L/L_{D_c}>1$).

The reliability of the above-mentioned scheme has been tested by performing a series of theoretical calculations for the relevant regions identified previously. We have found that the proposed scheme is essentially valid, except in the zones close to the lines separating the different regions, where intermediate behaviors have been observed. Representative examples concerning the Fano factor, γ, and the contributions into which it is decomposed, γ_P and γ_C, are shown in Figs. 7–10 for each of the five regions individuated in the $L-\mu$ plane.

Figure 7 displays the Fano factor for $L=5$ and $\mu=-5$ ($L/L_{D_c}=0.32$) corresponding to region (i) (continuous line) and for $L=0.5$ and $\mu=8$ ($L/L_{D_c}=0.71$) corresponding to region (ii) (dot-dashed line). In both cases the presence of space charge in the active region is nearly negligible, insufficient to originate a potential energy maximum large enough so as to lead to Coulomb suppression. Therefore, both regions are concerned with the absence of Coulomb correlations ($\gamma_C=1$). In region (i) Pauli correlations are absent ($\gamma_P=1$ for $V>3$), since $\mu=-5$ implies that carriers are injected at the contacts with energies $\varepsilon-\mu>3$, so that the

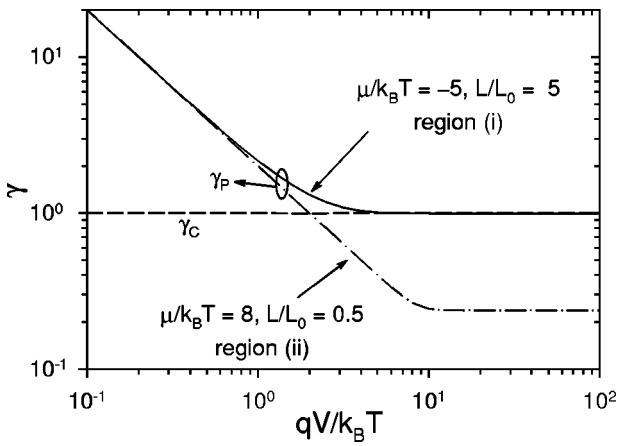

FIG. 7. Fano factor as a function of the applied voltage qV/k_BT for $L/L_0=5$ and $\mu/k_BT=-5$ corresponding to region (i) of Fig. 6 (solid line) and $L/L_0=0.5$ and $\mu/k_BT=8$ corresponding to region (ii) of Fig. 6 (dot-dashed line). Dashed line represents the Coulomb contribution to the Fano factor. By definition, in this case the Pauli contribution to the Fano factor is indistinguishable from the actual Fano factor.

distribution function at the contacts is well approximated by the nondegenerate Maxwell–Boltzmann distribution, and the injection statistics is Poissonian. On the contrary, in region (ii) Pauli correlations are responsible for the suppression of shot noise ($\gamma_P<1$ for $V>3$) since degenerate injection conditions prevail. It is worth noting that, in all cases where the long-range Coulomb correlations are absent, as in the present case, the Fano factor at low voltages decreases inversely with the applied bias according to the law

$$\gamma^{th}=\frac{2}{V}, \tag{41}$$

which corresponds to the thermal noise behavior, while at high voltages ($V>V_{cr}$) it becomes constant with a value given by

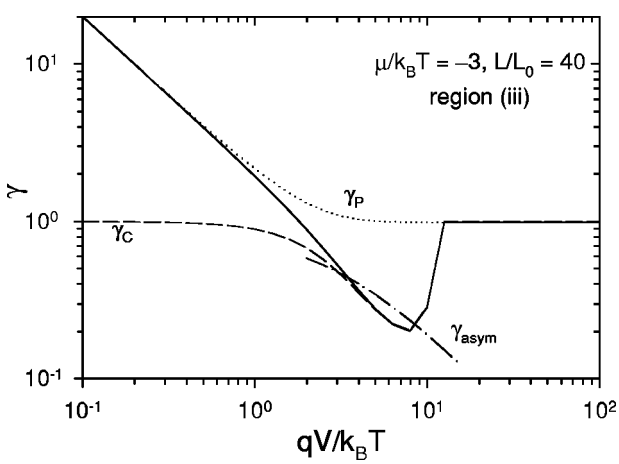

FIG. 8. Fano factor as a function of the applied voltage qV/k_BT for $L/L_0=40$ and $\mu/k_BT=-3$ corresponding to region (iii) of Fig. 6 (solid line). Dashed and dotted lines represent, respectively, the Coulomb and Pauli contributions to the Fano factor. Dashed-dotted line represents the results of the asymptotic theory.

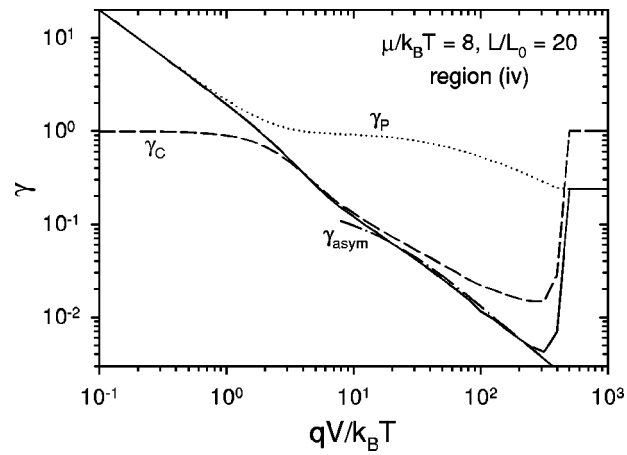

FIG. 9. Fano factor as a function of the applied voltage qV/k_BT for $L/L_0=20$ and $\mu/k_BT=8$ corresponding to region (iv) of Fig. 6 (solid line). Dashed and dotted lines represent, respectively, the Coulomb and Pauli contributions to the Fano factor. Dashed-dotted line represents the results of the asymptotic theory.

$$\gamma^{sat}=\frac{f_c(-\mu)}{\int_0^{+\infty} f_c(u-\mu)du}, \tag{42}$$

which corresponds to current saturation conditions. To obtain Eq. (42) use is made of Eqs. (16) and (34). The value of γ^{sat} interpolates monotonically between 1 for $\mu<-3$ (nondegenerate injection statistics) and $2/\mu$ for $\mu>3$ (strongly degenerate injection statistics). Since the Coulomb correlations vanish identically at thermal equilibrium and under current saturation conditions, the two limiting behaviors represented by Eqs. (41) and (42) are common to all cases, as we will see in the following.

Figure 8 reports the Fano factor for $L=40$ and $\mu=-3$ ($L/L_{D_c}=6.9$) corresponding to region (iii) of the general scheme. It shows the presence of Coulomb correla-

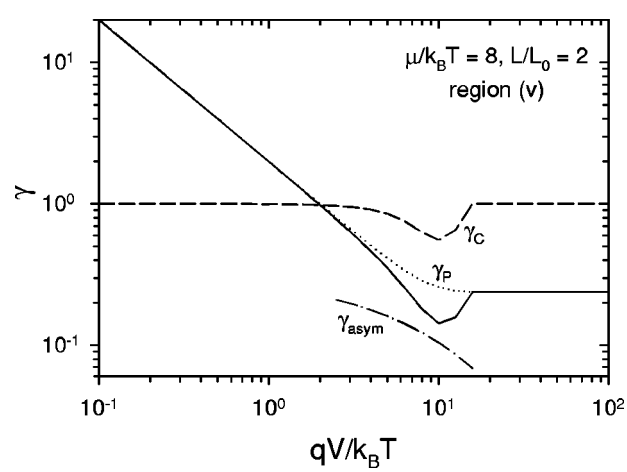

FIG. 10. Fano factor as a function of the applied voltage qV/k_BT for $L/L_0=2$ and $\mu/k_BT=8$ corresponding to region (v) of Fig. 6 (solid line). Dashed and dotted lines represent, respectively, the Coulomb and Pauli contributions to the Fano factor. Dashed-dotted line represents the results of the asymptotic theory.

tions ($\gamma_C<1$ for $3<V<V_{cr}$) and the absence of Pauli correlations ($\gamma_P=1$ for $V>3$). Pauli correlations are absent because $\mu=-3<0$ (see above), while Coulomb correlations set in due to relevant space charge effects. Due to the small value of the ratio L/L_{D_c} the asymptotic theory[22] provides only some rough agreement with the exact result in the limited range of voltages associated with a suppressed behavior. For larger values of the ratio L/L_{D_c} the agreement improves. The behavior displayed by the system in region (iii) was previously examined in detail in Ref. 18.

Figure 9 reports the Fano factor for $L=20$ and $\mu=8$ ($L/L_{D_c}=28.2$) corresponding to region (iv) of the general scheme. Here we assist to a low and intermediate voltage range where Coulomb correlations are dominating and to a high voltage range where Pauli correlations prevail. Indeed, the Fano factor displays the presence of Coulomb correlations ($\gamma_C<1$ for $3<V<V_{cr}$), the absence of Pauli correlations in an intermediate bias range ($\gamma_P\sim 1$ for $3<V\lesssim 10$), and the presence of Pauli correlations for higher bias ($\gamma_P<1$ for $V\gtrsim 10$). Physically, this behavior is due to the fact that in this region, even if contacts are under degenerate injection conditions ($\mu>0$), one has $\overline{U}_m^{eq}-\mu>0$, so that for the lowest applied voltages ($3<V\lesssim 10$) it is $\overline{U}_m-\mu>0$ and the current flows are only due to Poissonian carriers at the tail of the Fermi distribution function, leading to $\gamma_P\sim 1$. As V increases, it is $\overline{U}_m-\mu\leqslant 0$ and sub-Poissonian carriers near and below the Fermi level increasingly contribute to the current and low-frequency noise, so that Pauli correlations become manifest in the noise, thus leading to $\gamma_P<1$. Note that in region (iv) one generally has $L/L_{D_c}\gtrsim 10$, thus ensuring that the asymptotic theory[22] provides a good approximation to the exact theory presented here in the range of bias satisfying $U_m\ll V<V_{cr}$, as illustrated in Fig. 9.

Finally, Fig. 10 reports the Fano factor for $L=2$ and $\mu=8$ ($L/L_{D_c}=2.8$) corresponding to region (v) of the general scheme. The Fano factor displays the presence of both Pauli correlations ($\gamma_P<1$ for $V>3$) and Coulomb correlations ($\gamma_C<1$ for $3<V<V_{cr}$). In this region one always has $\overline{U}_m-\mu<0$, thus ensuring that Pauli correlations are present at all applied bias. Therefore, this is the most interesting region to analyze the interplay between Coulomb and Pauli correlations. We note that here the exact theory presented in this paper becomes strictly necessary, since in this region the ratio L/L_{D_c} never takes values much higher than unity (one typically obtains $1\lesssim L/L_{D_c}\lesssim 10$), thus reducing significantly the usefulness of the asymptotic theory,[22] as illustrated in Fig. 10.

To provide more insight into the interplay between Coulomb and Pauli correlations in region (v), Fig. 11 reports the Fano factor as a function of bias for $L=3$ and several values of μ belonging to region (v). It is observed that by increasing the value of μ the contribution of the Pauli correlations decreases faster than that of the Coulomb correlations. This is understood by noting that for $\mu>3$, γ_P varies as $2/\mu$, while γ_C, being determined by the ratio L/L_{D_c}, varies as $\sqrt{\mu}$. Physically, this behavior reflects the increasing amount of

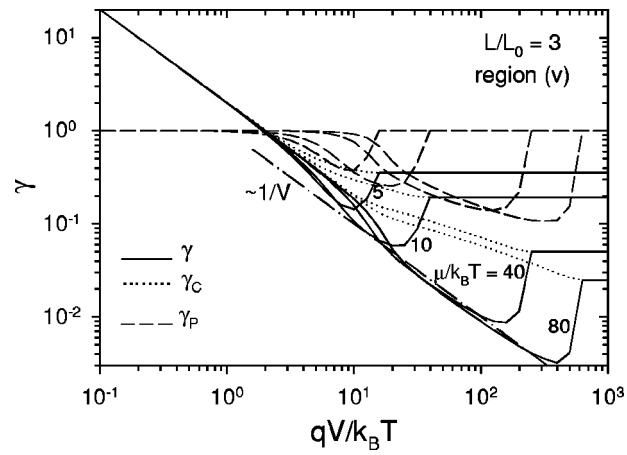

FIG. 11. Fano factor as a function of the applied voltage qV/k_BT for $L/L_0=5$ and several values of μ/k_BT corresponding to region (v) of Fig. 6 (solid line). Dashed and dotted lines represent, respectively, the Coulomb and Pauli contributions to the Fano factor. The dashed-dotted line gives the $1/V$ slope.

sub-Poissonian carriers contributing to the current as μ becomes higher. These carriers lead to a more and more pronounced Pauli suppression while they do not contribute so much to Coulomb suppression, since due to their sub-Poissonian character the fluctuations of U_m they induce are much less significant than those originated by the Poissonian carriers above the Fermi level. For this reason, γ_C tends to saturate for the highest values of $V<V_{cr}$ while γ_p continues decreasing. Remarkably enough, in region (v) for $V>30$ the total Fano factor γ is well described in all cases by a $1/V$ dependence. As seen in the figure, this dependence on voltage is due to the joint action of both Pauli and Coulomb correlations. It can also be observed that the onset of Coulomb suppression takes place for higher values of V as μ increases, since for this suppression to become significant it is necessary that the contribution to the current due to carriers injected at the right contact becomes negligible. This takes place when $V+\overline{U}_m\cong\mu$, a condition that requires a higher value of V as μ increases, for a given value of L.

To illustrate a realistic example where the theoretical results presented here could be applied, we consider as a significant example the case of a ballistic GaAs n^+-i-n^+ homodiode at $T=4$ K and contact density $n_c=1.14\times 10^{16}$ cm^{-3}. For this structure $k_BT/q=0.3$ mV, $\mu=8$ (0.24 meV), $L_0\sim 31$ nm and $L_{D_c}\sim 0.7$ (22 nm), where we have taken $m=0.066\ m_0$, and $\epsilon=12.9\,\epsilon_0$. For a sample length of 500 nm, $L\sim 16$, and according to Fig. 6 we are in region (iv) of the general scheme. For a sample length of 70 nm, $L\sim 2.3$ and we are in region (v). For a sample length of 15 nm, $L\sim 0.5$ and we are in region (ii). To explore regions (i) and (iii) one can refer to the case of heterodiodes.[31] We conclude that in principle the different behaviors of the Fano factor predicted by the present theory can be investigated experimentally within realistic conditions.

VI. CONCLUSIONS

We have presented a semiclassical theory of nonequilibrium noise (shot-noise) properties of n^+-i-n^+ ballistic semi-

conductor structures aimed at evaluating the relevance of the long-range Coulomb interaction and of the Pauli exclusion principle. The theory covers the whole range of system parameters, physically identified in the contact chemical potential, the sample length, and the applied voltage. Within a unitary scheme free from any approximation we succeed in investigating the transition between: nondegenerate and degenerate injection conditions, short and long sample lengths, and low and high applied bias. Through the determination of the Fano factor, we have analyzed the relevance of Coulomb and Pauli correlations. At applied voltages above about $3k_BT/q$ both correlations lead to the suppression of shot noise. We have identified five different regions in the plane defined by the sample length and the chemical potential corresponding, respectively, to the following conditions. (i) the absence of Pauli and Coulomb correlations; (ii) the presence of Pauli correlations and the absence of Coulomb correlations; (iii) the absence of Pauli correlations and the presence of Coulomb correlations; (iv) the absence (presence) of Pauli correlations for low (high) bias and the presence of Coulomb correlations; and (v) the presence of both Pauli and Coulomb correlations. Case (i) corresponds to small sample lengths and nondegenerate conditions when different current pulses are clearly uncorrelated. Case (ii) occurs for small sample lengths and degenerate injection conditions so that Pauli correlations are the only being active. Case (iii) implies a large sample length and nondegenerate injection conditions so that Coulomb correlations are the only being active. Case (iv) is associated with large samples and degenerate injection conditions. Here Coulomb correlations are always present because of the small value of the Debye screening length. In addition, at low bias only Poissonian carriers at the tail of the contact energy distribution contribute to the noise so that Pauli correlations are absent, while at higher bias Pauli principle becomes active due to the increasing amount of carriers obeying binomial injection statistics that contribute to noise. Finally, case (v) refers to moderately long samples and degenerate injection conditions so that both Coulomb and Pauli correlations are present simultaneously. The results of the theory are in perfect agreement with analogous MC simulations. Therefore, besides offering a complete physical picture of the subject, this study provides new insight into the noise properties of ballistic conductors, and of mesoscopic systems in general. We believe that the theory here developed constitutes a powerful tool to design experimental investigations of the nonequilibrium noise properties of solid-state ballistic conductors.

ACKNOWLEDGMENTS

Partial support from the DURSI of the Generalitat de Catalunya (Spain), the Consejería de Educación y Cultura de la Junta de Castilla y León through Project No. SA057/02, the Ministerio de Ciencia y Tecnología (Spain) through Project Nos. TIC2001-1754, BFM2000-0624, BFM2001-2159, and the Ramon y Cajal program, and from the Italy–Spain Joint Action of the MIUR Italy (Ref. IT-109) and MCyT Spain (Ref. HI2000-0138) is gratefully acknowledged.

APPENDIX: DERIVATION OF THE MAIN FORMULAS

Here we derive the main formulas used in the paper by following a procedure similar to that used in Ref. 18, here extended to the case of degenerate injection conditions. To this end, the first step consists in solving for the distribution function that satifies the Vlasov–Poisson–Langevin system of equations, Eqs. (1)–(9). To find the solution we first note that, since transport is ballistic, the total longitudinal energy of a carrier u, defined as

$$u=\tfrac{1}{2}v_x^2+U(x,t)=\varepsilon_x+U(x,t), \tag{A1}$$

remains constant during the flight of the carrier through the structure. Then, we note that, since transport is ballistic, carriers can reach a given point inside the structure either directly from the contacts or indirectly after reflection at the self-consistent potential barrier. Moreover, we can identify from which contact the carrier comes from. From these considerations it is easy to convince oneself that, in the low frequency limit of interest in the present paper, the distribution function solving the set of Eqs. (1)–(9) is given by

$$F(x,v_x,t) = \begin{cases} f_0(u,t) & U_0<u<\infty, \quad v_x>0, \quad 0<x<x_m \\ f_L(u,t) & U_m<u<\infty, \quad v_x<0, \quad 0<x<x_m \\ f_0(u,t) & U_0<u<U_m, \quad v_x<0, \quad 0<x<x_m \\ f_0(u,t) & U_m<u<\infty, \quad v_x>0, \quad x_m<x<L \\ f_L(u,t) & U_L<u<U_m, \quad v_x>0, \quad x_m<x<L \\ f_L(u,t) & U_L<u<\infty, \quad v_x<0, \quad x_m<x<L, \end{cases} \tag{A2}$$

where

$$f_0(u,t)=F[0,+\sqrt{2(u-U_0)},t], \tag{A3}$$

$$f_L(u,t)=F[L,-\sqrt{2(u-U_L)},t], \tag{A4}$$

with $F(0,v_x,t)$ and $F(L,v_x,t)$ being obtained through the boundary conditions in Eqs. (5) and (6). In the previous expression $U_m\equiv U_m(t)$ and $x_m\equiv x_m(t)$ refer to the value and location of the potential energy maximum, respectively, while U_0 and U_L correspond to the values of the potential energy at the contacts (note that, according to the boundary conditions assumed here, these values do not fluctuate).

Since Eq. (A2) depends on the value of the maximum potential energy, to completely determine the distribution function we need to derive the equation satisfied by the energy maximum. To this purpose, we first obtain an expression for the carrier density by performing the integral in Eq. (3) with the help of Eq. (A2). After some algebra one can show that the carrier density is given by

$$n(x,t)=\begin{cases} n^-[U(x,t),U_m;[f_0,f_L]] & 0<x<x_m \\ n^+[U(x,t),U_m;[f_0,f_L]] & x_m<x<L, \end{cases} \tag{A5}$$

where

$$n^-(U,U_m;[f_0,f_L])=\int_{U_m}^{+\infty}\frac{du}{\sqrt{2(u-U)}}[f_0(u,t)+f_L(u,t)]+\int_U^{U_m}\frac{du}{\sqrt{2(u-U)}}2f_0(u,t) \tag{A6}$$

and

$$n^+(U,U_m;[f_0,f_L])=\int_{U_m}^{+\infty}\frac{du}{\sqrt{2(u-U)}}[f_0(u,t)+f_L(u,t)]+\int_U^{U_m}\frac{du}{\sqrt{2(u-U)}}2f_L(u,t). \tag{A7}$$

In the previous equations the square brackets on the left-hand side mean a functional dependence. Now, by multiplying the Poisson equation, Eq. (2), by $\partial U(x,t)/\partial x$ and integrating with respect to x, it can be shown that the electric field $E(x,t)$ is given through

$$E(x,t)=\begin{cases} E^-[U(x,t),U_m;[f_0,f_L]] & 0<x<x_m \\ E^+[U(x,t),U_m;[f_0,f_L]] & x_m<x<L, \end{cases} \tag{A8}$$

with

$$E^-(U,U_m;[f_0,f_L])=\left\{\int_{U_m}^{\infty}du[\sqrt{u-U}-\sqrt{u-U_m}][f_0(u,t)+f_L(u,t)]+\int_U^{U_m}du\sqrt{u-U}2f_0(u,t)\right\}^{1/2}2^{3/4} \tag{A9}$$

and

$$E^+(U,U_m;[f_0,f_L])=-\left\{\int_{U_m}^{\infty}du[\sqrt{u-U}-\sqrt{u-U_m}]\times[f_0(u,t)+f_L(u,t)]+\int_U^{U_m}du\sqrt{u-U}2f_L(u,t)\right\}^{1/2}2^{3/4}. \tag{A10}$$

Finally, from the definition $\partial U(x,t)/\partial x=E(x,t)$ and its integration with respect to the space coordinate, we arrive at the following inverse equations for the potential energy profile

$$\int_{U_0}^{U^-(x,t)}\frac{dU}{E^-(U,U_m;[f_0,f_L])}=x, \tag{A11}$$

valid for $0<x<x_m$, and

$$\int_{U_L}^{U^+(x,t)}\frac{dU}{E^+(U,U_m;[f_0,f_L])}=x-L, \tag{A12}$$

valid for $x_m<x<L$.

From the previous expressions the location of the maximum energy potential can be obtained by evaluating either Eq. (A11) or Eq. (A12) at $x=x_m$,

$$\int_{U_0}^{U_m}\frac{dU}{E^-(U,U_m;[f_0,f_L])}=x_m, \tag{A13}$$

$$\int_{U_L}^{U_m}\frac{dU}{E^+(U,U_m;[f_0,f_L])}=x_m-L. \tag{A14}$$

By eliminating x_m from the two resulting equations we derive a closed equation for the value of the potential energy maximum in the form

$$L=\int_{U_0}^{U_m}\frac{dU}{E^-(U,U_m;[f_0,f_L])}-\int_{U_L}^{U_m}\frac{dU}{E^+(U,U_m;[f_0,f_L])}. \tag{A15}$$

Equation (A15) constitutes a closed equation to determine the value of the potential energy maximum, U_m. Notice that it depends solely on the boundary conditions for the distribution function and the sample length.

Once the value of the potential energy maximum is known, one can determine its location through either Eq. (A13) or Eq. (A14). Then, from Eq. (A2) one obtains the explicit expression of the distribution function. In a similar way the explicit spatial dependence of the potential energy can be determined by substituting the value of U_m in Eqs. (A11) and (A12), and that of the electric field and carrier density by substituting U_m in Eq. (A8) and Eq. (A5), respectively. In this way, a complete analytical solution of the model presented in Sec. III is obtained.

In particular, the electrical current, defined as

$$I(t)=-\int_{-\infty}^{+\infty}dv_xv_xF(x,v_x,t), \tag{A16}$$

can be shown to be given by

$$I(t)=\int_{U_m}^{+\infty}du[f_L(u,t)-f_0(u,t)]. \tag{A17}$$

Now, we are in the position to derive the corresponding expressions for the transport and noise properties.

1. Transport properties

The average steady-state transport properties can be computed directly from Eqs. (A5)–(A17) presented above by simply substituting into them

$$\begin{aligned} U_m &\to \overline{U}_m, \\ x_m &\to \overline{x}_m, \\ f_0(u,t) &\to \overline{f}_0(u)=f_c(u-\xi_0), \\ f_L(u,t) &\to \overline{f}_L(u)=f_c(u-\xi_L), \end{aligned} \tag{A18}$$

with $f_c(\varepsilon)$ given through Eq. (7). In this way we arrive at the equations used in Sec. IV A.

2. Low frequency current noise properties

The fluctuating properties of any of the quantities of interest can be evaluated directly from Eqs. (A5)–(A17) derived above by just performing the corresponding perturbation around the steady state, and by taking into account that the only source of fluctuations in the system is located at the contacts, and represented by the fluctuating term in Eq. (7). In this paper we are interested in the low frequency current fluctuations. To compute them we perturb Eq. (A17) around the steady state thus obtaining

$$\delta I(t)=\int_{\overline{U}_m}^{+\infty} du[\delta f_L(u,t)-\delta f_0(u,t)] -[\overline{f}_L(\overline{U}_m)-\overline{f}_0(\overline{U}_m)]\delta U_m(t), \tag{A19}$$

where $\delta U_m(t)$ represents the fluctuations of the potential energy maximum. In Eq. (A19) we distinguish two contributions to the current fluctuation, one coming directly from the contacts and the other coming indirectly through the self-consistent potential fluctuations. To express the dependence of the second contribution on the noise sources, we perturb Eq. (A15). In performing such a perturbation it is convenient to shift all the energy integration variables by an amount equal to U_m. After some algebra one then arrives at the following expression for the fluctuations of the maximum potential energy:

$$\delta U_m(t)=\frac{1}{\Delta}\int_{U_L}^{+\infty} du\,\tilde{\gamma}_L(u)\,\delta f_L(u,t) + \frac{1}{\Delta}\int_{U_0}^{+\infty} du\,\tilde{\gamma}_0(u)\,\delta f_0(u,t), \tag{A20}$$

with

$$\Delta=\frac{1}{\overline{E}_L}-\frac{1}{\overline{E}_0}+\int_{U_L}^{+\infty} du\,\tilde{\gamma}_L(u)\overline{f}_{\rm FD}(u-\xi_L) + \int_{U_0}^{+\infty} du\,\tilde{\gamma}_0(u)\overline{f}_{\rm FD}(u-\xi_0), \tag{A21}$$

where we have used that $\overline{f}_0'(u)=-\overline{f}_{\rm FD}(u-\xi_0)$ and $\overline{f}_L'(u)=-\overline{f}_{\rm FD}(u-\xi_L)$. Here, we have defined

$$\tilde{\gamma}_L(u)=\tilde{\gamma}^{>}(u)\,\theta(u-\overline{U}_m)+\tilde{\gamma}_L^{<}(u)\,\theta(\overline{U}_m-u), \tag{A22}$$

$$\tilde{\gamma}_0(u)=\tilde{\gamma}^{>}(u)\,\theta(u-\overline{U}_m)+\tilde{\gamma}_0^{<}(u)\,\theta(\overline{U}_m-u), \tag{A23}$$

with

$$\tilde{\gamma}^{>}(u)=\int_{U_0}^{\overline{U}_m}\frac{[\sqrt{2(u-U)}-\sqrt{2(u-\overline{U}_m)}]dU}{E(U,\overline{U}_m;[\overline{f}_0,\overline{f}_L])^3} -\int_{U_L}^{\overline{U}_m}\frac{[\sqrt{2(u-U)}-\sqrt{2(u-\overline{U}_m)}]dU}{E(U,\overline{U}_m;[\overline{f}_0,\overline{f}_L])^3}, \tag{A24}$$

$$\tilde{\gamma}_L^{<}(u)=\int_{U_L}^{u}\frac{-2\sqrt{2(u-U)}dU}{E^{+}(U,\overline{U}_m;[\overline{f}_0,\overline{f}_L])^3}, \tag{A25}$$

$$\tilde{\gamma}_0^{<}(u)=\int_{U_0}^{u}\frac{2\sqrt{2(u-U)}dU}{E^{-}(U,\overline{U}_m;[\overline{f}_0,\overline{f}_L])^3}. \tag{A26}$$

By substituting Eq. (A20) in Eq. (A19) for the current fluctuations we finally obtain

$$\delta I(t)=\int_{U_L}^{+\infty} du\,\gamma_L(u)\,\delta f_L(u,t) + \int_{U_0}^{+\infty} du\,\gamma_0(u)\,\delta f_0(u,t), \tag{A27}$$

with

$$\gamma_L(u)=\theta(u-\overline{U}_m)+\Omega\,\tilde{\gamma}_L(u), \tag{A28}$$

$$\gamma_0(u)=-\theta(u-\overline{U}_m)+\Omega\,\tilde{\gamma}_0(u), \tag{A29}$$

where

$$\Omega=-\frac{[\overline{f}_c(\overline{U}_m-\xi_L)-\overline{f}_c(\overline{U}_m-\xi_0)]}{\Delta}. \tag{A30}$$

Now we are in the position to compute the low frequency current spectral density, defined as

$$S_I(0)=\int_{-\infty}^{+\infty}\overline{\delta I(0)\,\delta I(t)}dt. \tag{A31}$$

By substituting Eq. (A27) into Eq. (A31) we arrive at

$$S_I(0)=\int_{\overline{U}_L}^{+\infty} du\,\gamma_L(u)^2 f_{\rm FD}(u-\xi_L) + \int_{\overline{U}_0}^{+\infty} du\,\gamma_0(u)^2 f_{\rm FD}(u-\xi_0), \tag{A32}$$

where we have used that from Eq. (9) one has

$$2\int_{-\infty}^{+\infty}\overline{\delta f_a(u,t)\,\delta f_{a'}(u',t')}dt' =f_{\rm FD}(u-\xi_a)\,\delta_{a,a'}\,\delta(u-u')\,\delta(t-t'). \tag{A33}$$

From Eqs. (A24) to (A32) it is straightforward to arrive at the equations used in Sec. IV B.

[1] Yu.V. Sharvin, Zh. Eksp. Teor. Fiz. **48**, 984 (1965); Sov. Phys. JETP **21**, 655 (1965).
[2] A.G.M. Jansen, A.P. van Gelder, and P. Wyder, J. Phys. C **13**, 6073 (1980).
[3] M. Heiblum, M.I. Nathan, D.C. Thomas, and C.M. Knoedler, Phys. Rev. Lett. **55**, 2200 (1985).
[4] A.F.J. Levi, J.R. Hayes, P.M. Platzman, and W. Weigmann, Phys. Rev. Lett. **55**, 2071 (1985).
[5] R. Trzcinski, E. Gmelin, and J.H. Queisser, Phys. Rev. B **35**, 6373 (1987).
[6] B.J. van Wees, H. van Houten, C.W. Beenakker, J.G. Williamson, and C.T. Fox, Phys. Rev. Lett. **60**, 848 (1988).
[7] W.J. Kaiser and L.D. Bell, Phys. Rev. Lett. **60**, 1406 (1988).
[8] M. Heiblum, D.C. Thomas, C.M. Knoedler and M.I. Nathan, Appl. Phys. Lett. **47**, 1105 (1985).
[9] A.F.J. Levi, J.R. Hayes, and R. Bhat, Appl. Phys. Lett. **48**, 1609 (1985).
[10] K. Natori, J. Appl. Phys. **76**, 4879 (1994).
[11] L.E. Wernersson, A. Litwin, L. Samuelson and H. Xu, IEEE Trans. Electron Devices **44**, 1829 (1997).
[12] Z.S. Gribnikov, N.Z. Vagidov, A.N. Korshak and V.V. Mitin, J. Appl. Phys. **87**, 7466 (2000).
[13] Ya.M. Blanter and M. Buttiker, Phys. Rep. **336**, 1 (2000).
[14] A. van der Ziel and G. Bosman, Phys. Status Solidi A **73**, K93 (1982).
[15] I.O. Kulik and A.N. Omel'yanchuk, Fiz. Nizk. Temp. **10** 305 (1984) [Sov. J. Low Temp. Phys. **10**, 158 (1984)].
[16] D.O. North, RCA Rev. **4**, 441 (1940); **5**, 106 (1941).
[17] T. González, O.M. Bulashenko, J. Mateos, D. Pardo, and L. Reggiani, Phys. Rev. B **56**, 6424 (1997); O.M. Bulashenko, J. Mateos, D. Pardo, T. González, L. Reggiani, and J.M. Rubí, *ibid.* **57**, 1366 (1998).
[18] O.M. Bulashenko, J.M. Rubí, and V.A. Kochelap, Phys. Rev. B **61**, 5511 (2000).
[19] Sh. Kogan, *Electronic Noise and Fluctuations in Solids* (Cambridge University Press, Cambridge, 1996).
[20] Y. Naveh, A.N. Korotkov, and K.K. Likharev, Phys. Rev. B **60**, R2169 (1999).
[21] T. González, J. Mateos, D. Pardo, and L. Reggiani, Physica B **272**, 285 (1999).
[22] O.M. Bulashenko and J.M. Rubí, Phys. Rev. B **64**, 045307 (2001).
[23] The effects of injection statistics that are an arbitrary function of energy and of fractional-type have also been addressed. See, for instance, O.M. Bulashenko, J.M. Rubí, and V.A. Kochelap, Phys. Rev. B **62**, 8184 (2000); G. Gomila and L. Reggiani, *ibid.* **63**, 165404 (2001).
[24] B. Brill and M. Heiblum, Phys. Rev. B **54**, R17 280 (1996).
[25] Z. Xie and S.A. Lyon, Appl. Phys. Lett. **75**, 2085 (1999).
[26] L.S. Levitov and G.B. Lesovik, Pis'ma Zh. Éksp. Teor. Fiz. **58** 225 (1993) [JETP Lett. **58**, 230 (1993)].
[27] T. González, J. Mateos, D. Pardo, L. Varani, and L. Reggiani, Semicond. Sci. Technol. **14**, L37 (1999).
[28] A. Greiner, L. Reggiani and L. Varani, Semicond. Sci. Technol. **15**, 1071 (2000).
[29] A. Van der Ziel, *Noise* (Prentice–Hall, New York, 1954).
[30] H. Nyquist, Phys. Rev. **32**, 110 (1928).
[31] O.M. Bulashenko, J.M. Rubí, and V.A. Kochelap, Appl. Phys. Lett. **75**, 2614 (1999).